Characterization of Microscopic Pore-Throat Structure of Tight oil Reservoir: a Case Study of C2 and C7 Section in Ordos Basin

Chunhua Lu[1,a], Hanqiao Jiang[1,b], Chengcheng You[1,c], Shiyuan Qu[1,d] and Junjian Li[1,e]

[1]China University of Petroleum, Beijing 102249, China
a. 1306801944@qq.com, b. 13125091108@163.com, c. 42638521@qq.com, d. 737251469@qq.com, e. 2350575409@qq.com

Keywords: Tight reservoirs, pore structure, pressure-controlled porosimetry, rate-controlled porosimetry.

Abstract: Understanding the pore structure of tight reservoirs is essential to improve the development of tight oil. In this paper, 12 cores in C2 and C7 section of Ordos Basin were subjected to pressure-controlled porosimetry (PCP) experiments and rate-controlled porosimetry (RCP) experiments to characterize the pore throat structure of tight cores. The results show that the pore radius varies from 100μm to 350μm with small difference. The throat controls the shape of the mercury intrusion curve and is the main storage space for tight sandstone, with radius less than 10μm. The combined PCP pore-throat radius curve and RCP throat radius curve show that when the radius is less than 0.12μm, the denser the core, the pore-throat shows similar properties to the throat on the mercury injection curve.

1. Introduction

With the decrease of conventional sandstone oil and gas resources, the exploration and development of tight reservoir has become the key point[1-3]. Rock is a place for fluid storage and seepage, and its physical properties directly control the productivity and ultimate recovery rate of oil and gas wells. Especially in tight reservoirs, the micro-nano-scale pore throat restricts the migration of oil and gas. So identifying the pore throat structure of the rock is a very meaningful job[4].

Existing pore structure characterization techniques include scanning electron microscopy (SEM)[5], nuclear magnetic resonance (NMR)[6], X-ray computer tomography (CT)[7, 8], mercury intrusion[9], etc. Although the SEM method can visualize the distribution of pore throats, it cannot quantitatively describe the size of pore throats[10]. The NMR method is mainly to saturate the core with crude oil, measure the relaxation time of the crude oil, and then convert the relaxation time into the size of the pore throat. The result is interfered by whether the saturated crude oil is sufficient and the water phase signal[11]. The CT method is limited due to the resolution of the instrument, it is impossible to characterize pores with a radius less than 65nm[12]. In this paper, PCP and RCP experiments were conducted on C2 and C7 low-permeability reservoirs in Ordos Basin, respectively, to describe the microscopic pore structure characteristics of tight reservoirs.

2. Reservoir Characteristics

The Ordos Basin is located in the central part of China with rich in oil and gas resources. The Yanchang Formation is one of its most important oil-bearing strata series, which has important research and economic value. It is characterized by wide oil and gas distribution, multiple oil-bearing layers, low permeability and low porosity[13]. Up to now, the ten sections (C1~C10) of Yanchang Formation are important oil-producing reservoirs in Ordos Basin. Among them, the C2 section is a delta plain subfacies deposit, with relatively developed sand bodies. The lithology is mainly gray-green and light gray silt sandstone with dark mudstone. Clay minerals are mainly chlorite, with a relative content of 74.32%. The content of illite and imonite mixed layers are similar, 13.51% of illite and 12.17% of imonite mixed layers. The average porosity is 18.43% and the average permeability. 39.28mD, belonging to a medium porosity and low permeability reservoir. The C7 section is mainly composed of lacustrine sedimentary system. Although delta system and turbidite system are also developed, the sand content is low.The clay mineral is mainly chlorite, but the content in the longer block 2 is low, which is 67.52%. The content of illite and Aemon mixed layer is 13.45% and 19.03%, respectively. The average porosity is 11.26% and the average permeability is 0.197mD, which belong to ultra-low permeability reservoir[14].

3. Experimental Sample

The basis of the PCP is the capillary bundle model. Since mercury does not wet the rock surface, additional pressure is needed to inject mercury into the rock pores. Therefore, the intrusion pressure is equivalent to the capillary pressure. The corresponding capillary radius is the pore-throat radius. The volume of mercury intrusion the pore is the pore-throat volume. The RCP is an advanced technology for the detection of rock microscopic pore structure characteristics. It injects mercury into the rock pores at a very low constant speed to keep the injection rate quasi-static. In the quasi-static process, every change in the shape of the pore experienced by the front edge of mercury will cause a change of the meniscus, thereby causing a change in the capillary pressure of the system. According to the pressure fluctuation characterized by the meniscus surface at the mercury inlet, the microstructure of the pores was determined and the pore and throat were separated. The test results can intuitively and quantitatively analyze the size and distribution characteristics of pores, throats, pore-throat radius ratios, etc. In this paper, 6 cores were selected from each of the C2 and C7 sections. The cores of C2 sections were x1, x1-1, x2, x2-1, x3, x3-1, and the cores of C7 were w1, w1-1, w2, w2-1, w3, w3-1, of which six cores x1, x2, x3, w1, w2, and w3 were subjected to PCP experiments, x1-1, x2-1, x3-1, w1-1, w2-1, w3-1 for RCP experiment. PCP was performed on a PoreMaster PM33-13 mercury porosimeter following the standard SY/T 5346-2005 of China. The instruments used are American corelab CMS300 and American AutoPore IV 9505 mercury porosimeter. The samples are dried at 105°C before testing, and the maximum experimental pressure is 200MPa. The American Coretest ASPE730 was used for RCP experiments. The inlet pump speed was set as 0.00005ml/min, and the final inlet pump pressure was 6.2MPa. The experimental results are shown in Table 1 and Table 2.

Table 1: Results of PCP experimental.

[a]Samples	Subsection	Poro(%)	Perm(mD)	P_t(MPa)	R_m(μm)	P_{50}(MPa)	R_{50}(μm)	Sorc	Effi(%)
w1	C7	15.89	0.26	0.27	2.72	1.86	0.40	2.94	35.77
w2	C7	14.46	0.21	0.42	1.75	2.04	0.36	2.90	31.23
w3	C7	10.83	0.15	0.48	1.53	2.78	0.26	2.82	33.71
x1	C2	17.37	36.72	0.05	13.87	0.15	4.77	3.14	27.24
x2	C2	19.67	54.16	0.06	13.36	0.25	2.94	3.44	23.86
x3	C2	18.75	21.61	0.05	13.61	0.22	3.34	3.38	25.21

[a] P_t, R_m, P_{50}, R_{50}, Sorc, Effi represent the threshold pressure, maximum pore-throat radius, medium saturation pressure, medium pore-throat radius, separation coefficient and extrusion efficiency, respectively.

Table 2: Results of CP experimental.

[b]Sample	Subsection	Poro(%)	Perm(mD)	Sf(%)	St(%)	Sb(%)	Rt(μm)	Rp(μm)
w1-1	C7	15.89	0.26	64.03	40.41	23.62	1.24	159.45
w2-2	C7	14.46	0.21	64.51	38.11	26.40	1.05	162.09
w3-1	C7	10.83	0.15	73.06	39.47	33.59	1.27	166.15
x1-1	C2	17.37	36.72	88.83	56.27	32.56	5.70	188.33
x2-1	C2	19.67	54.16	91.21	62.89	28.32	5.45	179.91
x3-1	C2	18.75	21.61	84.97	55.35	29.62	5.81	183.28

[b] Sf, St, Sb, Rt, Rp represent total mercury intrusion saturation, pore mercury saturation, throat mercury saturation, average radius of throat and average radius of pore, respectively.

4. Results

4.1.PCP Curves

The shape of a typical mercury intrusion curve can generally be divided into three sections: the initial section, the middle gentle section, and the end upturned section. The closer the curve is to the horizontal axis, the larger the core pore-throat radius, the flatter the smooth in the middle gentle section, the more concentrated the pore distribution of the core, and the better the pore throat sorting. The Figure 1 show that the middle gentle section of the mercury intrusion curve in C2 is closer to the horizontal axis, indicating that the C2 capillary pressure is lower than that of the C7 under the same mercury saturation. So the corresponding maximum pore-throat radius of C2 is 13.61μm, which is greater than 2.00μm of the C7. However, there is not much difference between the cores of the C2 and C7 at the end upturned section, indicating that the pore-throat separation of C2 is worse than that of C7. The average separation coefficient of three cores of C2 is 3.32, which is greater than 2.89 of C7, and the corresponding extrusion efficiency of the cores of C2 is also lower than that of C7(conclusions from Table1).

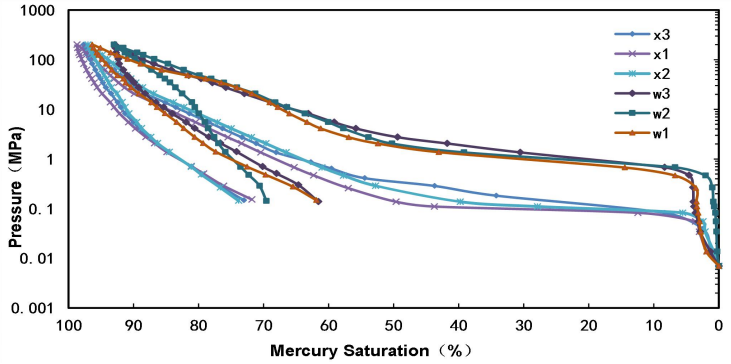

Figure 1: Intrusion and extrusion curves of PCP.

4.2.Pore Size Distribution by PCP

Pore size distribution curves were calculated on the basis of PCP intrusion curves using Washburn equation [15](Figure 2). The pore size of the three samples in the C2 section are mainly distributed between 1.5μm to 8.9μm, of which the x1 sample accounts for 58.7% of the interval, followed by x2, which accounts for 55.3% and 52.0% of the x3. The pore size of the samples in the C7 block are mainly distributed between 0.2μm to 1.1μm, and the corresponding proportions are 50.21% of w1, 51.85% of w2, and 44.84% of w3. 6 samples with pore-throats with a radius of less than 0.2μm are also well developed.

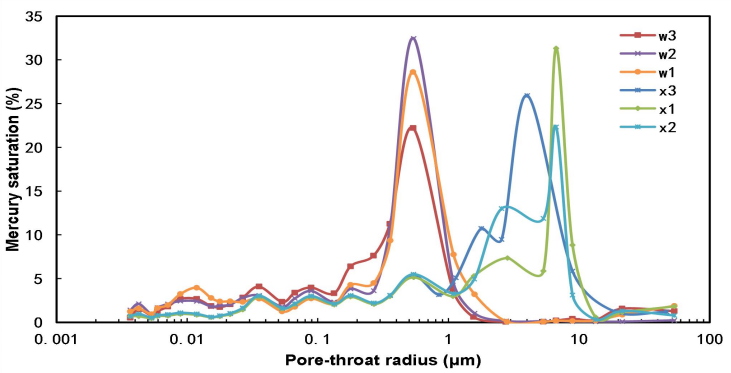

Figure 2: pore-throat size distribution by PCP.

4.3.RCP Curves

The advantage of the RCP is that the mercury intrusion curve of pore, throat and total can be obtained separately, so that pores and throats can be distinguished. It can be seen from Figure 3 that the curves of the two sections have a common feature: in the early stage of mercury intrusion, the mercury intrusion curves of total and pore have the same trend, which shows that the mercury saturation is mainly controlled by the pores. With the increase of mercury saturation, the pore mercury intrusion curve rises straight, indicating that the pores basically have no mercury ingress capacity. At this time, the total curve was mainly controlled by the throat. And the saturation of mercury in the throat was higher than that in the pores, indicating that the throat was the main storage space.

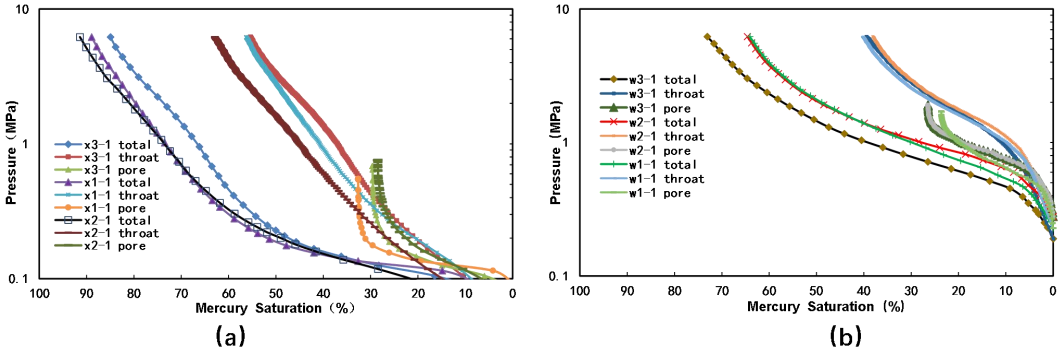

Figure 3: RCP curves of the total, pore and throat. (a) C2 section; (b) C7 section.

4.4.Pore and Throat Size Distribution by RCP

Figure 4 are the size distribution curves of the pores and throats respectively. From (a), we can see that the pore curves are similar in shape. The pore radius mainly develops between 100μm~350μm, but the peak of C2 is greater than that of C7. It can also be concluded from Table 2 that the average pore radius of the C2 is 183.84μm larger than the 162.57μm of the C7. The distribution of the throat radius is significantly different. For the C2 with larger permeability, the throat distribution interval is wider than the C7 and the peak value is smaller than the C7. From Table 2, the average of the C2 throat radius is 5.65μm greater than 1.19μm in C7.

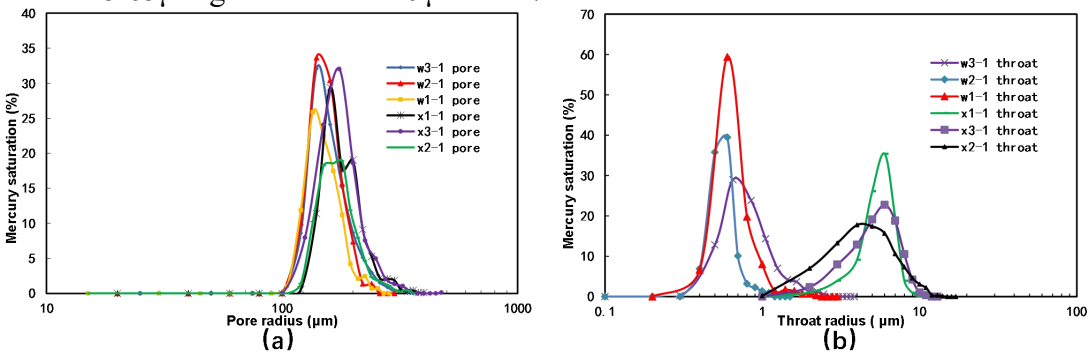

Figure 4: pore and throat size distribution by RCP. (a) pore; (b) throat.

5. Discussion

According to the results of RCP, the pore radius of C2 and C7 are all over 100μm, and the throats radius are less than 0.2μm. We guess that both the pore and throat show the properties of throat on RCP curve for that the pore and throat are of similar size at the nanoscale. In order to verify this hypothesis, the PCP curve and the throat curve of RCP are combined together. If the two curves coincide well at a radius close to 0.12 m, our hypothesis will be verified. The results of combined curve are shown in Figure 5.

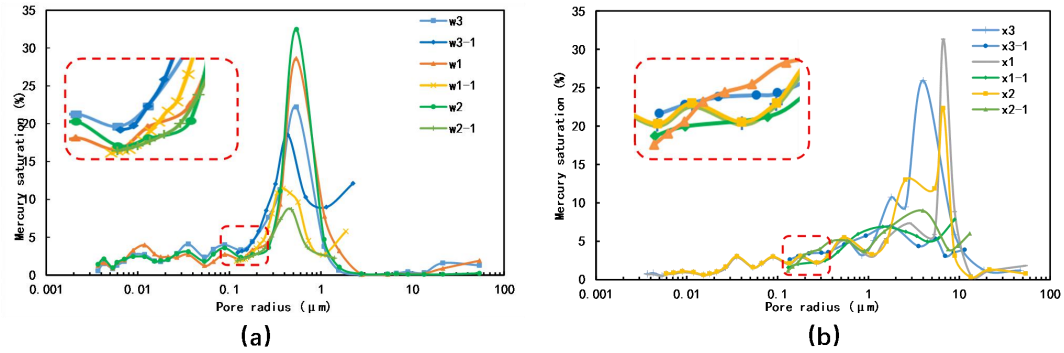

Figure 5: pore-throat size distribution by a combination of PCP and RCP. (a) C7 section; (b) C2 section.

It can be seen from Figure 5a that the PCP pore-throat radius distribution curve and the RCP throat radius distribution curve of the C7 overlap well at the radius less than 0.35μm, which shows that the throat is characterized by PCP. So when the radius is less than 0.12μm, the curve of Fig5a represents is still the throat.

The Figure 5b shows that the C2 has a large difference between the PCP pore-throat radius distribution curve and the RCP throat radius distribution curve. This is mainly due to the throat radius of the C2 samples are large, so the pore volume controlled by the large-throat is also large. At the same time, the distribution range of the throat radius is wide, leading to a large difference in pore volume, which is reflected in the PCP pore-throat radius distribution curve with multiple peaks. Even if the radius is around 0.12μm, there is still a difference in the combined curve, indicating that our hypothesis is not true in a reservoir with better physical properties

6. Conclusion

(1) The pore-throat radius of core of C2 is larger than that of C7, resulting in a smaller capillary force, and the corresponding curve of PCP is closer to the horizontal axis.

(2) The average value of the sample sorting coefficient of the C7 is 2.88, which is better than the 3.34 of the C2, making the difference of the pore-throat radius of the C7 sample smaller, so the extrusion efficiency is also higher.

(3) In RCP, the final mercury saturation of the pores is lower than the throat. The tight sandstone throat is the main storage space, and the total RCP curve is ultimately controlled by the throat.

References

[1] Zou, C.; Zhu, R.; Wu, S.; Yang, Z.; Tao, S.; Yuan, X.; Hou, L.; Yang, H.; Xu, C.; Li, D., Types, characteristics, genesis and prospects of conventional and unconventional hydrocarbon accumulations: taking tight oil and tight gas in China as an instance. Acta Petrolei Sinica 2012, 33, (2), 173-187.

[2] Miller, B. A.; Paneitz, J. M.; Mullen, M. J.; Meijs, R.; Tunstall, K. M.; Garcia, M. In The successful application of a compartmental completion technique used to isolate multiple hydraulic-fracture treatments in horizontal Bakken shale wells in North Dakota, SPE Annual Technical Conference and Exhibition, 2008; Society of Petroleum Engineers: 2008.

[3] Suyun, H.; Rukai, Z.; Songtao, W.; Bin, B.; Zhi, Y.; Jingwei, C., Exploration and development of continental tight oil in China. Petroleum Exploration and Development 2018, 45, (4), 790-802.

[4] Zhao, H.; Ning, Z.; Wang, Q.; Zhang, R.; Zhao, T.; Niu, T.; Zeng, Y., Petrophysical characterization of tight oil reservoirs using pressure-controlled porosimetry combined with rate-controlled porosimetry. Fuel 2015, 154, 233-242.

[5] Jiao, K.; Yao, S.; Liu, C.; Gao, Y.; Wu, H.; Li, M.; Tang, Z., The characterization and quantitative analysis of nanopores in unconventional gas reservoirs utilizing FESEM–FIB and image processing: an example from the

lower Silurian Longmaxi Shale, upper Yangtze region, China. International Journal of Coal Geology 2014, 128, 1-11.

[6] Zhao, P.; Wang, Z.; Sun, Z.; Cai, J.; Wang, L., Investigation on the pore structure and multifractal characteristics of tight oil reservoirs using NMR measurements: Permian Lucaogou Formation in Jimusaer Sag, Junggar Basin. Marine and Petroleum Geology 2017, 86, 1067-1081.

[7] Bin, B.; Rukai, Z.; Songtao, W.; Wenjing, Y.; Gelb, J.; Gu, A.; ZHANG, X.; Ling, S., Multi-scale method of Nano (Micro)-CT study on microscopic pore structure of tight sandstone of Yanchang Formation, Ordos Basin. Petroleum Exploration and Development 2013, 40, (3), 354-358.

[8] Zhou, G.; Zhang, Q.; Bai, R.; Ni, G., Characterization of coal micro-pore structure and simulation on the seepage rules of low-pressure water based on CT scanning data. Minerals 2016, 6, (3), 78.

[9] Feng, C.; Shi, Y.; Li, J.; Chang, L.; Li, G.; Mao, Z., A new empirical method for constructing capillary pressure curves from conventional logs in low-permeability sandstones. Journal of Earth Science 2017, 28, (3), 516-522.

[10] Desbois, G.; Urai, J. L.; Kukla, P. A.; Konstanty, J.; Baerle, C., High-resolution 3D fabric and porosity model in a tight gas sandstone reservoir: A new approach to investigate microstructures from mm-to nm-scale combining argon beam cross-sectioning and SEM imaging. Journal of Petroleum Science and Engineering 2011, 78, (2), 243-257.

[11] Lai, J.; Wang, G.; Fan, Z.; Chen, J.; Wang, S.; Zhou, Z.; Fan, X., Insight into the Pore Structure of Tight Sandstones Using NMR and HPMI Measurements. Energy & Fuels 2016, 30, (12), 10200-10214.

[12] Yao, Y.; Liu, D.; Che, Y.; Tang, D.; Tang, S.; Huang, W., Non-destructive characterization of coal samples from China using microfocus X-ray computed tomography. International Journal of Coal Geology 2009, 80, (2), 113-123.

[13] Yang, H.; Deng, X., Deposition of Yanchang Formation deep-water sandstone under the control of tectonic events in the Ordos Basin. Petroleum Exploration and Development 2013, 40, (5), 549-557.

[14] Tang, X.; Zhang, J.; Wang, X.; Yu, B.; Ding, W.; Xiong, J.; Yang, Y.; Wang, L.; Yang, C., Shale characteristics in the southeastern Ordos Basin, China: Implications for hydrocarbon accumulation conditions and the potential of continental shales. International Journal of Coal Geology 2014, 128, 32-46.

[15] Washburn EW. The dynamics of capillary flow. Phys Rev 1921; 17:273.